Available online at www.sciencedirect.com
SCIENCE DIRECT®
Journal of Solid State Chemistry 177 (2004) 3383–3391
JOURNAL OF SOLID STATE CHEMISTRY
http://elsevier.com/locate/jssc

$SrMn_3O_6$: an incommensurate modulated tunnel structure

L.J. Gillie,[a] J. Hadermann,[a] O. Pérez,[a,*] C. Martin,[a] M. Hervieu,[a] and E. Suard[b]

[a] *Laboratoire de cristallographie et sciences des materiaux, Ecole National Superieure d'Ingenieurs de Caen, UMR CNRS 6508, ISMRA-ENSICAEN, 6, boulevard du Marechal Juin, 14050 Caen Cedex, France*

[b] *Institut Laue Langevin, BP156, Avenue des Martkyrs, F38042 Grenoble Cedex, France*

Received 30 March 2004; received in revised form 25 May 2004; accepted 30 May 2004

Available online 20 July 2004

Abstract

The crystallographic structure of a mixed valent manganite $SrMn_3O_6$ with a 1D modulated structure is reported. The $SrMn_3O_6$ structure can be described with the basic subcell space group *Pnma* ($a=9.1334(5)$ Å; $b=2.8219(2)$ Å; $c=12.0959(7)$Å), but transmission electron microscopy revealed that the study of the real structure requires a 4D-formalism approach with superspace group $P2_1/a(\alpha\beta 0)00$ (unique axis *c*), with a modulation wave vector *q* having the approximate components ($0.52a^*+0.31b^*$). The crystallographic structure is closely related to those of $Na_xFe_xTi_{2-x}O_4$ and $Pb_{1.5}BaMn_6Al_2O_{16}$, comprising of unusual ''figure-of-eight''-shaped tunnels, made up of strings of edge- and corner-sharing $(Fe/Ti)O_6$ or $(Mn/Al)O_6$ octahedra, with the other cations situated in the tunnel cavities. Structural refinement was performed on X-ray and neutron powder diffraction data using the 4D formalism. All atoms in the crystal are affected by a displacive modulation wave, and a saw tooth function is employed to model the displacement and occupancy of the Sr sites. Magnetic susceptibility measurements reveal a sharp antiferromagnetic transition with $T_N \sim 46$ K.

Keywords: Manganese oxides; Tunnel structures; Modulated structure; Neutron powder diffraction; High-resolution electron microscopy

1. Introduction

The magneto-electronic properties of transition metal oxides have long been the focus of scientific investigations, with one particular significant discovery being magnetoresistance in cubic (or pseudo-cubic) manganese-based perovskites [1–3]. The effect of an applied magnetic field on electrical resistivity was reported by Jonker and Van Santen [4,5] in the 1950s, but only over the last 15 years has research in this area become particularly prevalent.

Mixed valent (Mn^{3+}/Mn^{4+}) manganite phases with generic formula $Ln_{1-x}A_xMnO_3$ (Ln = lanthanide; A = divalent cation) initially formed the majority of materials studied, exhibiting a marked drop in the electrical resistivity upon application of a magnetic field and an insulator-to-metal transition near the ferromagnetic Curie temperature, T_C. The large magnitude of field required (several Tesla) renders these materials unsuitable for commercial applications in magnetic data storage. However, the report by Moritomo et al. [6] of low-field magnetoresistive properties in a double-layered Ruddlesden–Popper material $La_{1.2}Sr_{1.8}Mn_2O_7$ (less than 1 T) has resulted in many new perovskite-derived ''layered'' materials being synthesized and studied [7–14].

Naturally occurring manganese oxides show a wealth of structural variety and are not derived from the perovskite crystallographic structure, some examples of which are hollandite-type, ramsdellite, cryptomelane, psilomelane and pyrolusite. In some cases, they exhibit a mixed valent oxidation state for the manganese cations. Several of these and other related materials such as $Ba_6Mn_{24}O_{48}$ [15–17] form complex tunnel structures in which the cations that occupy the tunnels are often subjected to displacements and agitations which result in modulated and sometimes incommensurate structures.

The $SrMnO_{3-x}$–Mn_3O_4 phase diagram, studied by Negas and Roth in the 1970s [18,19], evidenced a

*Corresponding author. Fax: +33-2-31-95-16-00.
E-mail address: olivier.perez@ismra.fr (O. Pérez).

0022-4596/$ - see front matter © 2004 Elsevier Inc. All rights reserved.
doi:10.1016/j.jssc.2004.05.057

material with composition $SrMn_3O_6$, of which the crystallographic structure has never been solved to date. The A–Mn–O systems (where A = Ca, Sr or Ba) [20–24] have been researched by numerous groups, owing to the interesting electronic properties and abundance of crystallographic structures observed. A calcium analog $CaMn_3O_6$ has also been reported, but again no crystal structure has yet been published [21].

In this paper, we present the results of a study on an incommensurate 1D modulated form of $SrMn_3O_6$ which has a tunnel structure similar to that of $Na_xFe_xTi_{2-x}O_4$ [25,26] and $BaPb_{1.5}Mn_6Al_2O_{16}$ [27] (Fig. 1). A framework built up of ribbons of edge-sharing MnO_6 octahedra, corner-linked to neighboring ribbons, forms double tunnels with a "figure-of-eight" shape, in which the Sr^{2+} cations are located. An Sr/Mn ratio of 1:3 can be related to the ideal composition $SrMn_2O_4$ by considering the formula $Sr_{0.67}X_{0.33}Mn_2O_4$, wherein X represents a vacancy on the Sr site, thus leading to a structure in which 67% of the tunnel sites are filled with Sr^{2+} cations.

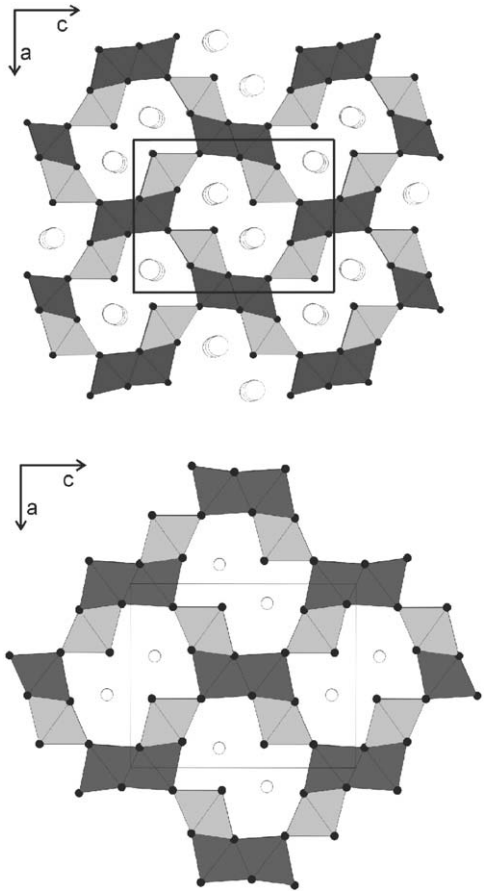

Fig. 1. Crystallographic structures of (a) $Na_xFe_xTi_{2-x}O_4$, and (b) $BaPb_{1.5}Mn_6Al_2O_{16}$, projected along the b-axis. Octahedra are Fe/TiO_6 and Mn/AlO_6 units and white circles represent Na and Ba/Pb cations in the tunnels. Octahedra at $y \sim 0.25$ and $y \sim 0.75$ are indicated by light and dark gray polyhedra, respectively.

2. Experimental

Stoichiometric proportions of SrO_2, Mn_2O_3 and Mn (1:1:1) were intimately ground in an agate mortar to achieve a homogeneous powder. This mixture was compacted into bars and placed into a recrystallized alumina finger and sealed in an evacuated silica tube, which was heated to 1200°C for 12 h and then slowly cooled to ambient temperature.

The phase purity was checked by X-ray diffraction (XRD) (Philips vertical diffractometer with Cu$K\alpha$ radiation, over a 2θ range of 10–70° with a step size of 0.02° over 2 h) and transmission electron microscopy (TEM). The phase purity check by TEM and the reconstruction of reciprocal space were carried out on a JEOL 2010 microscope, the high-resolution electron microscopy (HREM) study was performed with a TOPCON 002B microscope; both instruments are equipped with an energy-dispersive spectroscopy (EDS) analyser. Calculated HREM images were made using the MacTempas software. A more precise data set was collected by XRD (5–100° over 12 h) so that a starting point model could be deduced with reference to the heavier Mn and Sr cations. Neutron powder diffraction (NPD) data were collected on the high-resolution D2B instrument at the Institut Laue-Langevin, Grenoble ($\lambda = 1.594$ Å with Ge monochromator) and were subsequently refined using the JANA2000 package [28]. Magnetic susceptibility data were measured on a Quantum Design SQUID DC magnetometer. Both zero-field cooled and field-cooled data sets were collected in an applied field of 100 G.

3. Results and discussion

3.1. TEM study

Electron diffraction observations of the material revealed the presence of a main phase with ED patterns as shown in Fig. 2. On these patterns, the reflections can be divided into two groups. The most intense reflections are the basic reflections, which correspond to the *Pnma* subcell with $a = 9.1334(5)$ Å, $b = 2.8219(2)$ Å and $c = 12.0959(7)$ Å. The weaker reflections are satellite reflections due to an incommensurate modulation of the structure, with modulation vector $q \approx 0.52a^* + 0.31b^*$. When indexing these patterns using this modulation vector as the fourth basic vector, one gets the expression $s^* = ha^* + kb^* + lc^* + mq$ for the diffraction vector s^*, in which the reflections with $m = 0$ correspond to the basic reflections, and those with $m \neq 0$ to the satellite reflections. The electron diffraction (ED) patterns in Fig. 2 are indexed using this four-coordinate scheme. The q vector is indicated with an arrow, and the first- and second-order satellites of the 0 0 0 and 2 1 0

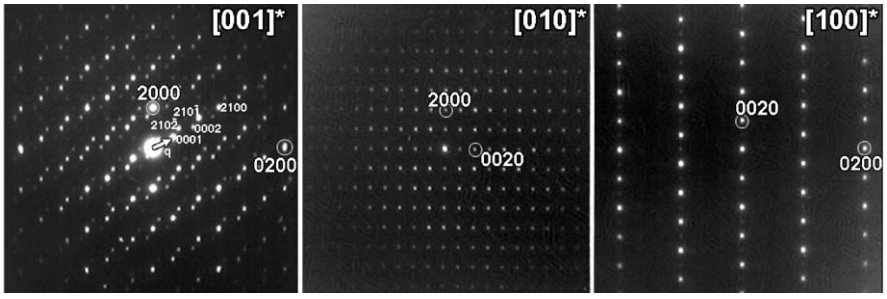

Fig. 2. Electron diffraction patterns of the main zones of $SrMn_3O_6$.

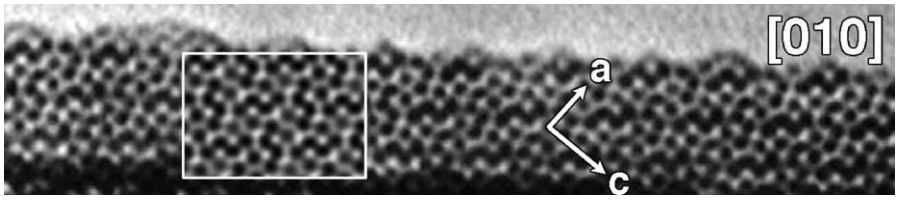

Fig. 3. HREM image along the [010] direction. Dark dots within white double loops are the tunnels with Sr atoms. The remaining dark dots correspond to the Mn atoms.

reflections are indicated for better understanding. The reflection conditions deduced from the ED patterns are $hk0m : h = 2n$ and $00l0 : l = 2n$, which leads to the super space group $P2_1/a(\alpha\beta0)$, with unique axis c.

Secondary phases were present as small domains within the crystals of the main phase. These secondary phases differed only in slightly different values for α and β, while all are in agreement with the same super space group $P2_1/a(\alpha\beta0)$. For instance, the following q^* wave vectors are observed: $q^* = 0.66a^* + 0.33b^*$ or $q^* = 0.56a^* + 0.28b^*$. The presence of these secondary phases hindered obtaining a unique value for the EDS measurements of the composition of the main phase. However, even though an exact value cannot be given, it was invariably found that the Mn to Sr ratio was higher than 3, indicating the presence of Sr vacancies compared to the ideal $SrMn_3O_6$ composition.

HREM images were made of the main phase and are shown in Figs. 3 and 4, along the [010] and [001] directions, respectively. On both experimental HREM images, calculated images are shown indicated by a white border. For these simulations, the commensurate model with parameters $2a$, $3b$ and c as described in the text hereafter was used. Excellent agreement between the calculated and experimental image was obtained at a defocus value of $\Delta_f = -30$ nm and thickness $t = 2$ nm for the image along the [010] direction (Fig. 3), and at values $\Delta_f = -25$ nm and $t = 12$ nm for the [001] image (Fig. 4). A shift of the modulation in the calculated image compared to that of the experimental one for the [001] image is due to the commensurate nature of the model and the incommensurate one of the real structure.

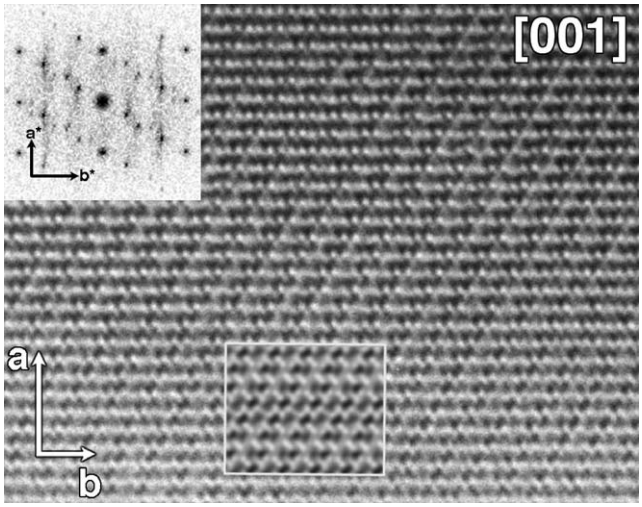

Fig. 4. HREM image along the [010] direction. Black and dark gray elongated dots on the calculated image in the white rectangle represent pairs of Sr atoms. The Fourier transform of the image is shown in the top left corner.

On the image along the [010] direction one can see double loops, arranged along two perpendicular directions, the dark dots in these loops depict the tunnels filled with Sr atoms, which are also part of the basic structure. The remaining black dots represent the projection along Mn columns. On the [001] image, the incommensurate modulation is clearly seen. All elongated black dots going from the bottom left to top right on the calculated image are pairs of Sr atoms, the darker as well as the grayer ones. The Mn atoms occur around

these Sr atoms on the white parts of the image. The correspondence with the ED patterns in Fig. 2 is seen more easily on the Fourier transform of the HREM image, which has been inserted on the top left corner of the image.

3.2. Refinement procedure

$SrMn_3O_6$ exhibits an incommensurately modulated structure. For these types of structures, the ratio between the period of the subcell and the one of the modulations is irrational; the 3D periodicity of the crystals is then lost. Two methods can be used to solve such a structure. Firstly, choosing a super cell approximation, for instance ($2a$, $3b$, c) and a low symmetry, a classical crystallographic study can be performed. Nevertheless, the large number of introduced parameters disturbs the refinement. Moreover, due to the loss of the 3D periodicity, such processing leads only to an average structure. Secondly, an accurate phase description can be obtained using the super space formalism, developed by De Wolff [29,30]; this approach is the only rigorous one. The super space formalism allows us, via the introduction of a fourth dimension, perpendicular to the three other ones, to recover the lost periodicity; then, tools of classical crystallography can be generalized for higher dimension space. Each atom is characterized by an average position $\langle r0 \rangle$ and an atomic displacement U and/or an occupancy P, expanded in Fourier series of the internal parameter x_4; these parameters are characteristic of the average structure and of the modulation, respectively. The expression of displacements U and occupancy P are the following:

$$U_i(\bar{x}_4) = \sum_n A_{i,n} \cos(2n\pi\bar{x}_4) + B_{i,n} \sin(2n\pi\bar{x}_4),$$

$$i = x,\ y,\ \text{or}\ z,$$

$$P(\bar{x}_4) = \langle P \rangle + \sum_n A_n \cos(2n\pi\bar{x}_4) + B_n \sin(2n\pi\bar{x}_4).$$

The average structure is calculated using only the main reflections, while the Fourier terms are mainly sensitive to satellites.

Both X-ray and neutron powder diffraction data are available to solve the $SrMn_3O_6$ structure. The contrast observed for Sr, Mn and O atoms depends on the radiation used. Thus, Sr and Mn are considered as "heavy" atoms for X-ray due to the value of their scattering factor in comparison with that of oxygen; a preliminary model, limiting the influence of O atoms, can be considered more easily than with neutron diffraction data.

Pattern-matching analysis was first performed on X-ray data using the cell parameters and the q wave vector found by the electron diffraction study as a starting point ($a = 9.25$ Å, $b = 2.87$ Å, $c = 12.09$ Å, $\alpha = \beta = \gamma = 90°$, $q = 0.52a^* + 0.31b^*$). The agreement factor on the profile is equal to 9.4%. Afterwards, profile parameters will be fixed to the obtained values. Let us emphasize that satellite reflections are clearly observed on the X-ray diffraction pattern. This suggests that the "heavy" atoms, i.e. Sr and Mn, are affected by the modulation.

A model based on the structure determined for $BaPb_{1.5}Mn_6Al_2O_{16}$ [27] was introduced in the refinement program Jana2000 [28]. The average structure was then refined. Strontium vacancies were evidenced; the site occupancy is close to roughly 2/3. Using all the reflections (main and satellite reflections), a starting model for the modulation is determined; small displacements along x, y and z were applied to the Sr atom. The sign of these displacements is tested via a trial and error method. An occupancy modulation is then introduced for Sr, which is very significant. With this first model established, displacement parameters were considered for Mn and O atoms. Satellites were calculated up to the second order. It has been verified that generated satellite reflections correspond to observed reflections. The agreement factors are equal to 12.5% on the profile (R_p), 5.1% on the main (R_0), 7% and 7.4% for first (R_1) and second (R_2) order satellite reflections.

Once the pattern matching procedure was performed, the previously refined structure was used as starting point for the study of the neutron diffraction data. The refinement is stable and leads to the following R factors:

$$R_p = 4.3\%,\ R_0 = 2.9\%,\ R_1 = 3.7\%,\ R_2 = 3.8\%.$$

These factors are very low, but, as for the X-ray study, two features in the modelization of the Sr(1) site must be clarified. Firstly, very large atomic displacements (± 0.85 Å) are evidenced along the b direction. Secondly, the model chosen for the occupancy induces a random distribution of the vacancies; it is indeed not possible to generate empty or fully occupied sites using Fourier series expansion up to the second order. As shown in the observed Fourier map calculated around the position expected for Sr(1) (Fig. 5), our model presents some defaults. Thus, the large displacements are linked to the particular shape of the undulated atomic string representing the Sr(1) site along x_4. It is discontinuous and exhibits alternatively a "hole" and two maxima along x_4. According to this observation, two strontium sites, with different y and x_4 positions, were introduced in place of the previous one (Fig. 5). Their existence domains along x_4, Δ_1 and Δ_2 are chosen to avoid overlap (Fig. 6). Moreover, the sum $\Delta_1 + \Delta_2$ is considered to be inferior to one; ordered strontium vacancies are then implied. Saw tooth functions are used to describe the displacement of the two strontium atoms. These functions are characterized by linear displacements along x, y and z and an existence domain centered on an $x_{4,0}$ value. No changes are observed for the

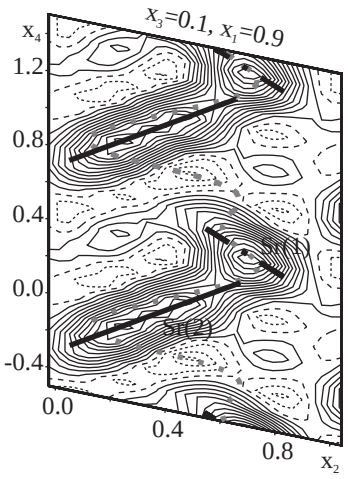

Fig. 5. Observed Fourier maps calculated around the expected strontium position. The gray dotted line corresponds to the harmonic model refined in the first refinement step (single strontium site) and dark segments to the final refinement step (alternative existence of Sr(1) and Sr(2) strontium site).

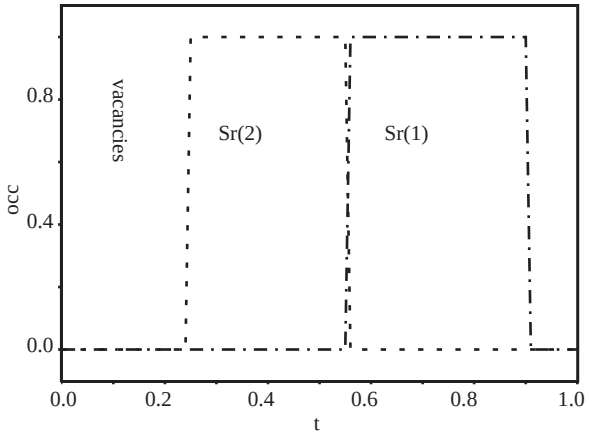

Fig. 6. Sr(1), Sr(2) and vacancies distribution versus t.

agreement factors, but this new model leads to perfect order for strontium and vacancies in the structure (Fig. 5). Results of the refinement are summarized in Table 1; observed and calculated neutron diffraction patterns are drawn in Fig. 7. The refined cell parameters are: $a = 9.1354(3)$ Å, $b = 2.8225(1)$ Å, $c = 12.1006(4)$ Å, $\alpha = \beta = \gamma = 90°$, $q^* = 0.5139(8)a^* + 0.3028(3)b^*$.

3.3. Structural analysis

As previously explained in the refinement section, $SrMn_3O_6$ is closely related to $BaPb_{1.5}Mn_6Al_2O_{16}$. The structure can then be described by edge-sharing MnO_6 octahedra, which exist in groups of four, in a distorted z-shape. These z-shaped units form an infinite ribbon along the short b-axis of the unit cell, and are corner-linked to four other z-shaped units to give double tunnels shaped like a figure of eight. The Sr cations are located in 67% of the available tunnel sites. In Fig. 1, the Mn cations located at $y \sim 0.25$ and $y \sim 0.75$ are indicated by dark and light polyhedra, respectively. The structure is heavily distorted but exhibits the same basic structural features of the non-stoichiometric phase $Na_xFe_xTi_{2-x}O_4$ [25,26]. The only reported Mn-containing tunnel structure of this type to date is that of $BaPb_{1.5}Mn_6Al_2O_{16}$ [27], which has exactly the same framework of metal-oxygen octahedra with Mn and Al statistically distributed over the octahedral sites. Interestingly, this material is reported to have a super-cell with a volume 10 times greater than the sub-cell (*Pnma*, $a = 9.219$ Å; $b = 2.828$ Å; $c = 12.113$ Å); however, there is no further analysis or discussion of this superstructure.

Let us now discuss the results obtained for the modulated structure. The existence of two extreme polyhedral types, octahedra and square-based pyramids, shown by the variation of the Mn–O bond lengths (Fig. 8), can be considered as the main effect of the modulation on the framework. Pyramidal geometry is adopted for Mn cations wherein one of the Mn–O bond lengths is significantly elongated relative to the other five bond lengths, and the octahedrally co-ordinated cations exist in more or less undistorted environments. In order to describe in the simplest manner how the modulations affect the polyhedral geometries of the manganese cations and the subsequent strontium distribution in the tunnel sites (Fig. 9), a super-cell was chosen with lattice parameters equivalent to $(2a + 3b + c)$. Fig. 10 shows the stacking of the Sr–Mn–O slices along b and a projection of these slices in the (a, c) plane; MnO_x co-ordination has been considered as pyramidal or more or less distorted octahedral. Note that the refined model of the anionic framework is independent of the choice of polyhedra; this discussion only affects the overall pictorial representation of the structure. $SrMn_3O_6$ could still be depicted as being built up of a uniquely octahedrally co-ordinated framework, but this would imply that Mn–O distances superior to 2.3 Å were considered to be reasonable and results in extremely distorted and unrealistic octahedra.

The actual structure is more complicated than it first seems as there are many Mn–O distances that can be assigned as being an "intermediate case geometry." In this case, there is no distinct cut-off point at which one can denote a manganese cation as being in either a five or six co-ordinate environment as there are several unreasonable distances; the corresponding MnO_6 octahedra are indicated in dark gray (Fig. 11). The main effect of the modulation on the framework is to re-approach the ideal $Na_xFe_xTi_{2-x}O_4$ model relative to the distorted $BaPb_{1.5}Mn_6Al_2O_{16}$.

The framework described above defines two types of tunnels, where Sr cations are inserted. The refinement results clearly show that the Sr sites are 67% occupied

Table 1
Atomic parameters (average and displacement parameters) and occupancy parameters

Name	Harmonic	x	y	z	U_{iso} (Å)
Mn(1)	$\langle\,\rangle$	0.0156(5)	0.233(4)	0.6089(4)	0.005(2)
	B_1	*	*	−0.0029(15)	
	A_1	*	−0.019(7)	−0.0035(14)	
	B_2	*	*	0.005(2)	
	A_2	−0.004(3)	*	*	
Mn(2)	$\langle\,\rangle$	0.6938(6)	0.25	0.3308(4)	0.007(4)
	B_1	−0.009(2)	−0.020(8)	−0.0046(15)	
	A_1	0.008(2)	*	0.0058(13)	
	B_2	0.013(2)	−0.020(10)	0.004(2)	
	A_2	0.006(3)	*	−0.005(2)	
Sr(1)	$\langle\,\rangle$	0.8396(10)	0.687(8)	0.0809(9)	0.005(3)
	U	*	−0.145(10)	*	
	$x_{4,0}/\Delta_1$	0.435(8)	0.269(11)		
Sr(2)	$\langle\,\rangle$	0.8466(10)	0.363(7)	0.0944(8)	0.005(3)
	U	*	0.313(16)	*	
	$x_{4,0}/\Delta_2$	*	0.341(11)		
O(1)	$\langle\,\rangle$	0.5921(4)	0.269(3)	0.1718(3)	0.010(1)
	B_1	−0.0094(12)	*	−0.0066(9)	
	A_1	−0.0082(13)	*	*	
O(2)	$\langle\,\rangle$	0.1745(4)	0.236(3)	0.7176(3)	0.0098(10)
	B_1	−0.0037(13)	*	0.0073(9)	
	A_1	0.0016(12)	0.016(5)	0.0120(7)	
O(3)	$\langle\,\rangle$	0.9096(4)	0.226(2)	0.9003(3)	0.010(1)
	B_1	−0.0140(10)	−0.002(5)	0.0056(9)	
	A_1	*	*	0.0097(8)	
O(4)	$\langle\,\rangle$	0.3841(4)	0.264(3)	0.0309(2)	0.0097(11)
	B_1	−0.0138(10)	−0.017(5)	0.0055(9)	
	A_1	−0.0015(14)	0.010(6)	0.0010(11)	

A_i, B_i, U, $x_{4,0}$, Δ_1 and Δ_2 are described in Section 3.2. *Non-significant and then fixed during the refinement to 0.

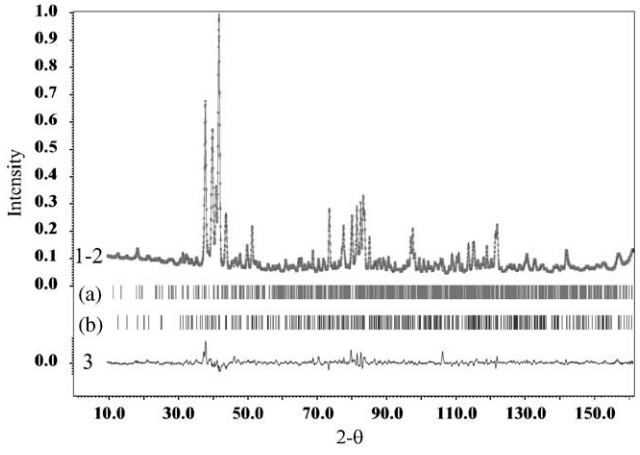

Fig. 7. Neutron diffraction patterns: observed (1), calculated (2) and difference (3) curves are drawn. Bragg positions for first-order satellite (a) and main (b) reflections are shown using vertical segments.

overall, which is in agreement with the Sr deficiency determined by EDS analysis. The Sr modulation occupancy allows us to locate the Sr cations and the vacancies in these tunnels. This modulation can be identified as the main one.

Infra-red (IR) measurements evidenced the presence of ca. 3% carbonate incorporated into the bulk of the material. By XRD, it would be unreasonable to expect the presence of these carbonate groups to be observed due to the light nature of the elements involved. Moreover, the percentage of carbonate detected inside our $SrMn_3O_6$ sample is very weak so that even by means of NPD the chance to evidence these groups is low. It should be noted that the refinement showed no evidence of the oxycarbonate $Sr_5Mn_4CO_3O_{10}$ [31] as an impurity phase. Carbonate insertion is expected within the double tunnels. These tunnels are partially occupied by Sr cations in which diluted Sr regions have been evidenced. These regions are then geometrically compatible with the presence of CO_3^{2-} groups. Difference Fourier maps were examined for the presence of residual unassigned electron density; however, as expected, no significant regions were revealed. Therefore, due to the good fit from the refinement, we have concluded that although

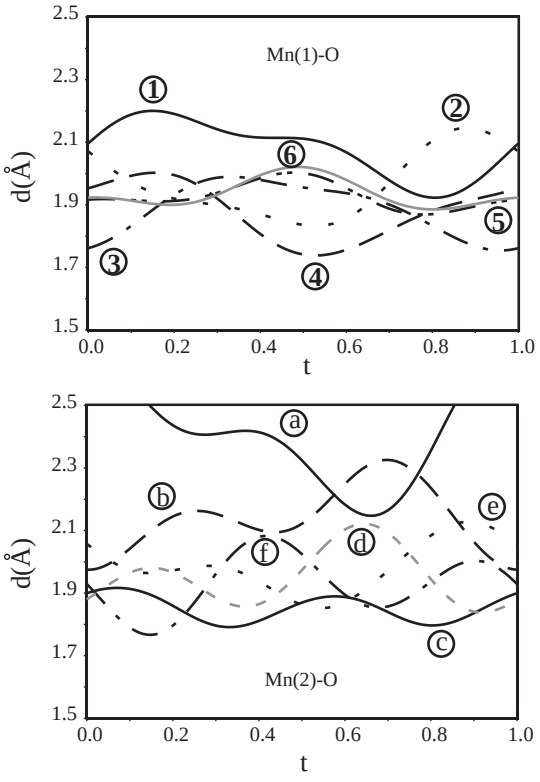

Fig. 8. Variation of Mn–O distances versus t. (1) Mn(1)–O(4) $(-1/2+x, y, 1/2+z, t)$, (2) Mn(1)–O(2), (3) Mn(1)–O(1) $(1/2-x, -y, 1/2-z, -t)$, (4) Mn(1)–O(1) $(1/2-x, 1-y, 1/2-z, -t)$, (5) Mn(1)–O(4) $(1/2-x, -y, 1/2-z, -t)$, (6) Mn(1)–O(4) $(1/2-x, 1-y, 1/2-z, -t)$, (a) Mn(2)–O(4) $(1/2+x, y, 1/2+z, t)$, (b) Mn(2)–O(1), (c) Mn(2)–O(3) $(3/2-x, -y, -1/2-z, -t)$, (d) Mn(2)–O(3) $(3/2-x, 1-y, -1/2-z, -t)$, (e) Mn(2)–O(2) $(1-x, 1-y, 1-z, -t)$, (f) Mn(2)–O(2) $(1-x, y, 1-z, -t)$.

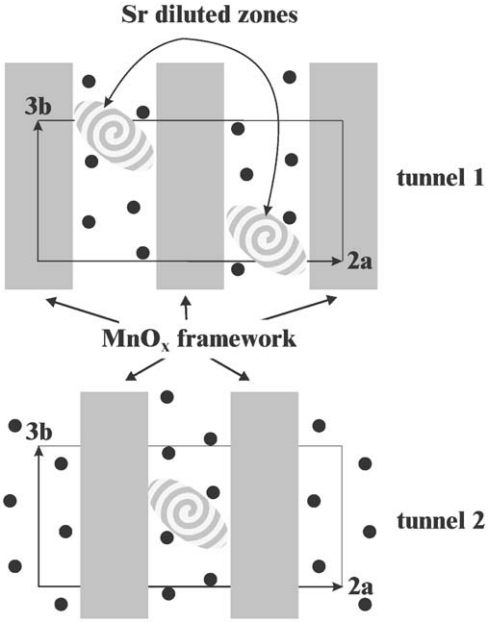

Fig. 9. Cross-section of the tunnels 1 and 2 indicating the strontium distribution. Strontium diluted zones are evidenced. Dark gray polyhedra correspond to distorted octahedra.

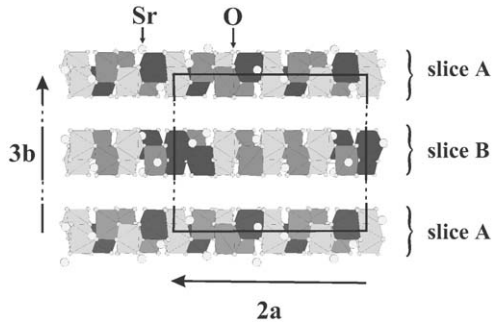

Fig. 10. Structural projection of $SrMn_3O_6$ along c. The model is expanded along b and the A, B, A slices are shown. Dark gray polyhedra correspond to distorted octahedra.

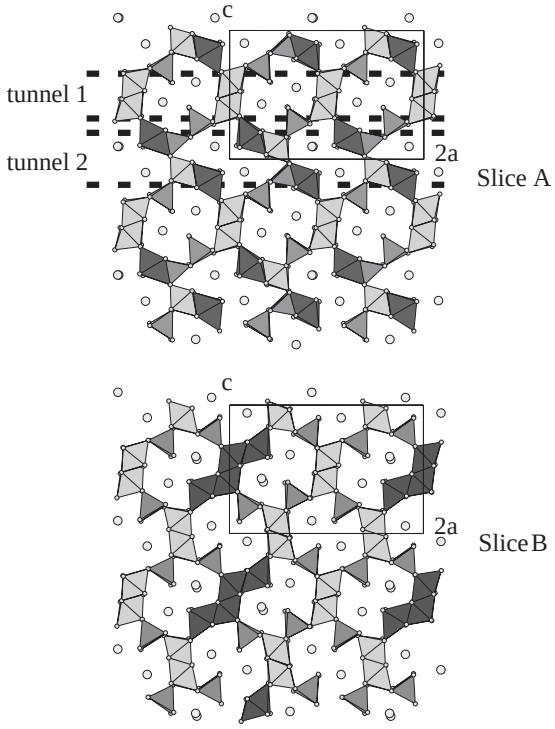

Fig. 11. Structural projection along b of the slices A and B. Dark gray polyhedra correspond to distorted octahedra.

there is evidence to suggest that there are carbonate groups incorporated into the bulk of this $SrMn_3O_6$ material, it is probable that they are randomly distributed within the figure-of-eight-shaped tunnels. However, another possibility for CO_3^{2-} insertion can be proposed: they could be located in place of Sr cations. But, due to the very comparable values of scattering lengths for C and Sr, this hypothesis is impossible to prove. The question of whether the incorporation of CO_3^{2-} groups into this phase plays a role in the stabilization of this particular structure has yet to be answered.

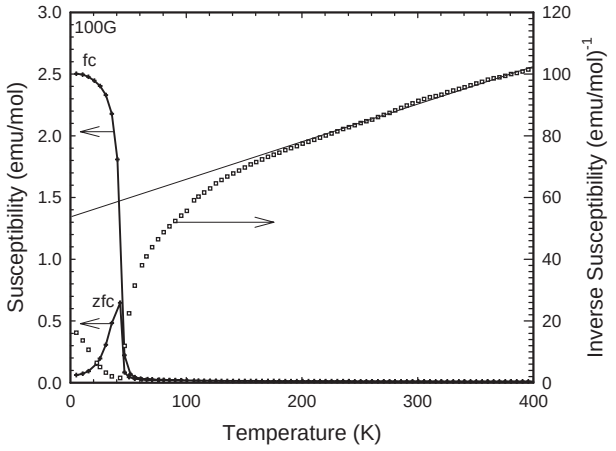

Fig. 12. Magnetic susceptibility versus temperature. Measurement performed in an applied field of 100 Oe (left axis) and inverse magnetic susceptibility versus temperature (right axis). Solid line represents linear fit between 200 and 400 K.

Calculated images were made based on this commensurate model to test it against the HREM images. These calculations are described in the TEM part.

3.4. Magnetic measurements

Magnetic susceptibility data reveal an antiferromagnetic transition at ca. 46 K; additionally, some ferromagnetic aspect to the behavior is also present as evidenced by the field-cooled data-set, indicated by triangles (Fig. 12). The inverse susceptibility can be fitted linearly by the Curie–Weiss law at higher temperatures (200–400 K), which equates to a paramagnetic moment of $4.76\mu_B$ per Mn cation (Fig. 13). It is close to the expected value ($4.54\mu_B$) of spin-only moment for manganese in an oxidation state between $+3$ ($d^4 = 4.87\mu_B$) and $+4$ ($d^3 = 3.89\mu_B$) according to the "ideal" formula $Sr(Mn_2^{3+}Mn^{4+})O_6$. The low θ_p value (≈ -450 K) shows the existence of strong AFM interactions of this compound. Further investigation by low-temperature NPD is required to determine the exact magnetic state. This will form part of a continuing study into this phase.

4. Summary

A new strontium manganite phase has been synthesized and characterized by structural refinement of NPD data using the 4D formalism. $SrMn_3O_6$ exhibits an average distorted tunnel structure with the same basic features as $Na_xFe_xTi_{2-x}O_4$ and $BaPb_{1.5}Mn_6Al_2O_{16}$, but a complicated incommensurate 1D modulation is present with modulation wave-vector components $q^* = 0.52a^* + 0.31b^*$. The existence of ordered strontium vacancies is implied from the structural refinement and this constitutes the main driving force of the modulation in $SrMn_3O_6$; the slight distortion of the Mn–O framework can be attributed to this ordering of strontium and vacancies. It could therefore be proposed that the $BaPb_{1.5}Mn_6Al_2O_{16}$ may also exhibit a similar type of modulation since the tunnel sites are again only partially occupied.

Acknowledgments

The authors thank the European Union for fellowships to L. Gillie and J. Hadermann (SCOOTMO: HRPN-CT-2002-00293 and SUPER-GMR: HPRN-CT-2000-0021 respectively). Authors are indebted to Prof. Marco Daturi for infra-red measurements.

References

[1] A.P. Ramirez, J. Phys.: Condens. Matter 9 (1997) 8171–8199.
[2] Y. Tokura, Y. Tomioka, J. Magn. Magn. Mater. 200 (1999) 1–23.
[3] B. Raveau, A. Maignan, C. Martin, M. Hervieu, Chem. Mater. 10 (1998) 2641–2652.
[4] G.H. Jonker, J.H. Van Santen, Physica 16 (1950) 337–349.
[5] G.H. Jonker, J.H. Van Santen, Physica 16 (1950) 599–600.
[6] Y. Moritomo, A. Asamitsu, H. Kuwahara, Y. Tokura, Nature 380 (1996) 141.
[7] P.D. Battle, M.J. Rosseinsky, Curr. Opin. Solid State Mater. Sci. 4 (2) (1999) 163–170.
[8] A.M. Abakumov, M.G. Rozova, B.Ph. Pavyluk, M.V. Lobanov, E.V. Antipov, O.I. Lebedev, G. Van Tendeloo, D.V. Sheptyakov, A.M. Balagurov, F. Bourée, J. Solid State Chem. 158 (2001) 100–111.
[9] A.M. Abakumov, M.G. Rozova, B.Ph. Pavyluk, M.V. Lobanov, E.V. Antipov, O.I. Lebedev, G. Van Tendeloo, O.L. Ignatchik, E.A. Ovtchenkov, Yu.A. Koksharov, A.N. Vasil'ev, J. Solid State Chem. 160 (2001) 353–361.
[10] A.J. Wright, H.M. Palmer, P.A. Anderson, C. Greaves, J. Mater. Chem. 11 (2001) 1324–1326.
[11] A.J. Wright, H.M. Palmer, P.A. Andersonl, C. Greaves, J. Mater. Chem. 12 (2002) 978–982.
[12] P.D. Battle, A.M. Bell, S.J. Blundell, A.I. Coldea, D.J. Gallon, F.L. Pratt, M.J. Rosseinsky, C.A. Steer, J. Solid State Chem. 167 (2002) 188–195.
[13] P.D. Battle, S.J. Blundell, P.N. Santhosh, M.J. Rosseinsky, C. Steer, J. Phys.: Condens. Matter 14 (2002) 13569–13577.
[14] L.J. Gillie, H.M. Palmer, A.J. Wright, J. Hadermann, G. Van Tendeloo, C. Greaves, J. Phys. Chem. Solids 65 (1) (2004) 87–93.
[15] J-P. Parant, R. Olazcuaga, M. Devalette, C. Fouassier, P. Hagenmuller, J. Solid State Chem. 3 (1971) 1–11.
[16] Ph. Boullay, M. Hervieu, B. Raveau, J. Solid State Chem. 132 (1997) 239–248.
[17] X.-J. Wu, Y. Fujiki, Acta Crystallogr. A 47 (1991) 405–413.
[18] T. Negas, J. Solid State Chem. 7 (1973) 85–88.
[19] T. Negas, R.S. Roth, J. Solid State Chem. 1 (1970) 409–418.
[20] B.L. Chamberland, A.W. Sleight, J.F. Weiher, J. Solid State Chem. 1 (1970) 506–511.
[21] H.S. Horowitz, J.M. Longo, Mater. Res. Bull. 13 (1978) 1359–1369.
[22] G.B. Ansell, M.A. Modrick, J.M. Longo, K.R. Poeppelmeier, H.S. Horowitz, Acta Crystallogr. B 38 (1982) 1795–1797.

[23] P.D. Battle, T.C. Gibb, C.W. Jones, J. Solid State Chem. 74 (1988) 60–66.
[24] K.J. Lee, E. Iguchi, J. Solid State Chem. 114 (1995) 242–248.
[25] W.G. Mumme, A.F. Reid, Acta Crystallogr. B 24 (1968) 625–631.
[26] A. Kuhn, F. Garcia-Alvarado, E. Moran, M.A. Alario-Franco, U. Amador, Solid State Ion. 86–88 (1996) 811–818.
[27] A. Teichert, Hk. Mueller-Buschbaum, J. Alloys Compds. 202 (1993) 37–40.
[28] V. Petriček, M. Dusek, Jana2000—The Crystallographic Computing System, Institute of Physics, Praha, Czech Republic, 2000.
[29] P.M. De Wolff, Acta Crystallogr. A 30 (1974) 777.
[30] P.M. De Wolff, T. Jansen, A. Janner, Acta Crystallogr. A 37 (1981) 625.
[31] V. Caignaert, B. Domengès, B. Raveau, J. Solid State Chem. 120 (1995) 279–289;
V. Caignaert, B. Domengès, B. Raveau, Acta Crystallogr. B 38 (1982) 1795–1797.